Wideband SiGe down-converter for millimeter-wave radio astronomy applications

Alireza Seyfollahi,[a,b,]* Nianhua Jiang[◉,a,b] Lewis B. G. Knee[◉,a]
and Jens Bornemann[◉b]
aNational Research Council Canada, Victoria, British Columbia, Canada
bUniversity of Victoria, Department of Electrical and Computer Engineering,
Victoria, British Columbia, Canada

Abstract. A Q-band down-converter module with high conversion gain (CG) is presented for a wideband radio astronomy receiver. This down-converter module is designed on a silicon-germanium (SiGe) heterojunction bipolar transistor (HBT) process ($0.13~\mu$m) to realize high CG, low LO power operation, and wideband frequency impedance matching for RF/LO/IF ports. The down-converter consists of a double-balanced Gilbert mixing core with on-chip RF/LO transformer baluns, an IF buffer, and bandpass filter. The performance of the down converter is largely dependent on the passive components and signal line interconnection. The design of all passive structures is analyzed and optimized with FEM simulations for a high-quality factor to minimize losses and parasitic effects. This module achieves 8 dB of CG at a low LO power of -6 dBm over a wide RF bandwidth from 28 to 56 GHz and IF bandwidth from 6 to 18 GHz. It demonstrates LO-to-IF/LO-to-RF/RF-to-IF isolations $>$ dB$/40$ dB/35 dB, respectively. The critical FEM simulation is described in the design of this high-density SiGe HBT RF circuit. The measured performance confirms the simulation results. The module meets the original design requirements of the DVA-2 Q-band receiver. © *2022 Society of Photo-Optical Instrumentation Engineers (SPIE)* [DOI: 10.1117/1.JATIS.8.3.036004]

1 Introduction

Large radio telescope arrays, such as the Atacama large millimeter/submillimeter array (ALMA)[1] or the proposed next-generation very large array (ngVLA),[2] image radio emission from astronomical objects by employing low noise radio receivers in different frequency bands.

In millimeter-wave receivers, the achievable IF bandwidth is usually a small fraction of the RF bandwidth. Therefore, a superheterodyne architecture is employed in this project to down-convert RF frequency slices to the IF. (Note that for submillimeter waves, LNAs are difficult to fabricate and, therefore, superconductor-insulator-superconductor mixers technologies are used.) It is desirable to increase the bandwidth of both RF and IF of each individual receiver without sacrificing performance. Increasing the RF bandwidth of each receiver reduces the number of bands required to cover a frequency-resolved spectrum. Based on the radiometer equation, a wider IF bandwidth corresponds to higher signal to noise ratio, hence higher receiver sensitivity in continuum observations. Both result in decreasing production and operation costs, and system complexity. The Dish Verification Antenna 2 (DVA-2), shown in Fig. 1, is a Canadian radio telescope built to demonstrate the capability of composite radio telescopes for high-frequency operation into the millimeter-wave range up to about 50 GHz.[3,4] The Q-band receiver design utilizes a heterodyne architecture where the 35–50 GHz RF spectrum is divided into two 8-GHz sub-bands, 35–43 GHz and 42–50 GHz for each of two polarizations. Each sub-band is down-converted to an 8–16 GHz IF suitable for digital processing. The DVA-2 Q-band

---
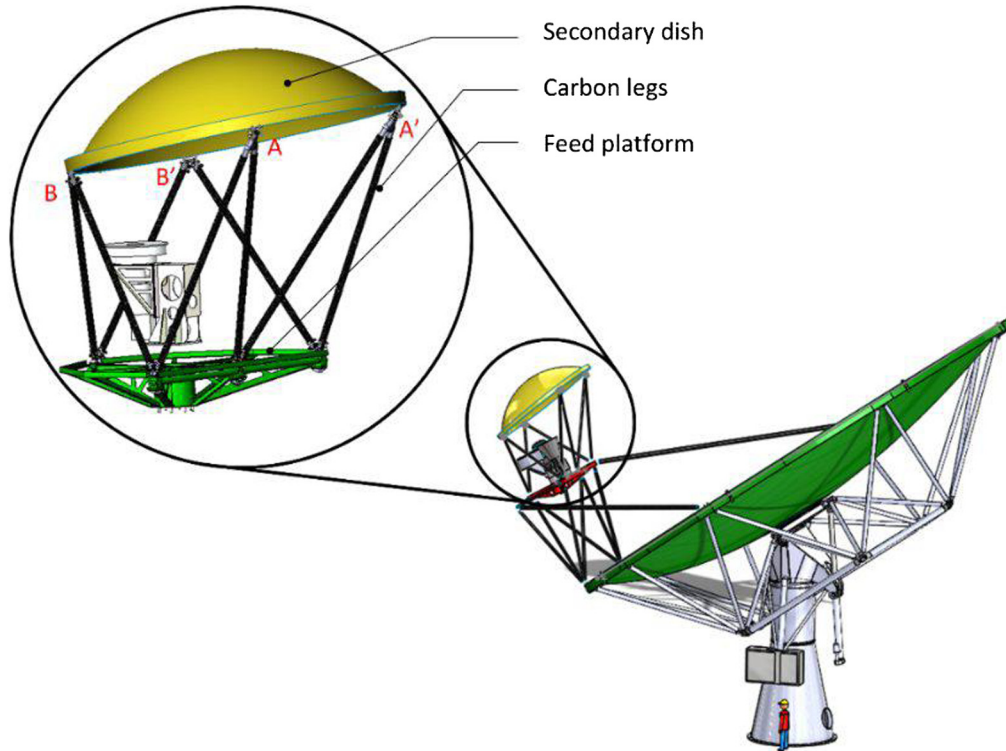
Fig. 1 DVA-2 radio telescope; CAD drawing from Ref. 3. Inset shows the secondary reflector and receiver platform.

Table 1 System noise temperature of the Q-band receiver for DVA-2 Telescope.

Freq. (GHz)	T_{Rx} (K)	T_{soill} (K)	T_{sky} (K)	η_{feed} (K)	T_{sys} (K)	T_{sys}/η_{feed} (K)
35	20.1	4.1	13.5	0.78	36.5	46.8
40	19.5	4.1	17.5	0.79	40.4	51.5
45	20	4.1	30.6	0.79	53.4	67.4
50	20	4.1	70.2	0.81	99.1	121.9

receiver design was a precursor for an ongoing development project at NRC[5] targeted toward a design for the ngVLA band 5 receiver.[6]

Table 1 lists in detail[5] the general system noise temperature requirement at different frequencies for the telescope that are calculated using ngVLA sky and spillover noise temperatures, which shows the required receiver noise temperature of better than 20 K. This directly affects the low noise amplifier (LNA) noise and gain requirements.

1.1 Background

The overall radio receiver noise is governed by Friis equation where to achieve a low noise temperature, the signal must be amplified using a high gain low noise amplifier, usually cryogenically cooled, followed by a warm amplifier to make the signal immune to loss/noise of the rest of the receiver chain including the down-converting mixer. The characteristics of the down-converter affect the system architecture components before and after the mixer in the chain.

Ideally, the mixer should be able to cover the entire RF band with acceptable input return loss, a consistent conversion gain (CG), and high isolation. The high CG can relax the cryogenic LNA/warm RF amplifier gain requirement. The down-converter design presented in this paper

has better CG and better input match compared with mixers offered in Refs. 7–10. In the case of conversion loss (typically somewhere between 0 and 10 dB), an IF amplifier is necessary to achieve the required accumulative gain for the entire receiver chain. Moreover, if the isolations between different ports of the mixer are <30 dB, isolators must be used at RF and IF ports of the mixer. The isolator is also needed if the input matching at RF and IF ports of the mixer is not at least better than 10 dB (which is a commonly accepted value from which on standing waves between mixer and RF/IF amplifiers are negligible).

It is important to note that unlike the LO and RF leakage to the IF path, the LO-to-RF leakage cannot be readily resolved by using a filter. The LO and RF frequencies are close and are only a few GHz apart in the millimeter-wave frequency band, and the LO frequency range overlaps the RF frequency band. Thus, a fixed frequency filter is not practical for tunable LO operation. A common method is using subharmonic mixers,[11,12] where the RF and LO subharmonics are separated from each other and the LO to RF leakage can be suppressed by using a simple filter. However, such mixers require high LO power and are associated with large conversion loss. Moreover, if the mixer provides adequate LO-to-IF isolation, the external band pass filter can be removed in some cases from the receiver, resulting in fewer components required.

Another important factor that mixers presented in Refs. 12–14 lack is the capability of operating with a minimum LO power. Those designs require at least 0 dBm LO power to operate properly to provide conversion loss of better than 15 dB. A down-converter system that operates with lower LO power is beneficial, especially in large array radio telescope systems. A 1 dB difference in LO power may seem small in a linearly polarized single dish telescope but it becomes significant when multiplied by the number of polarizations, sub-bands, bands, and antennas of a large array of radio telescopes. The capability of operation with low LO power reduces the complexity of the LO distribution system, especially in large telescope arrays with hundreds of receivers.

Figure 2(a) shows a simplified block diagram of a conventional radio receiver chain where many isolators and amplifiers are used after the low noise amplifier to prevent LO signals from leaking back to the antenna and disturbing adjacent receivers as well as reducing the standing
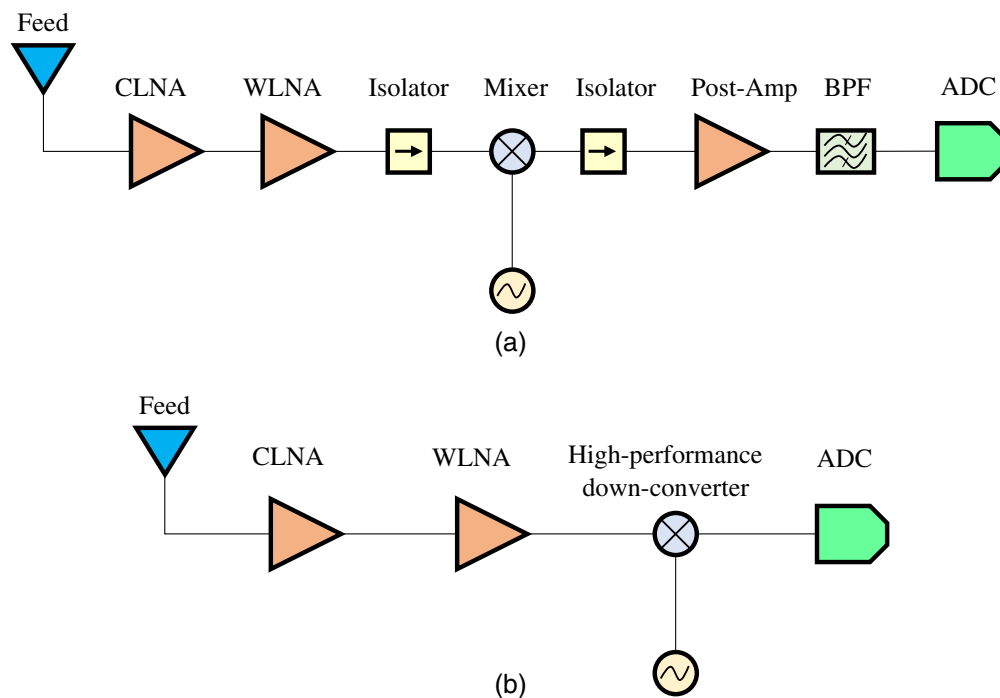
Fig. 2 (a) System block diagram of a typical superheterodyne radio receiver front end, with isolators and bandpass filters. (b) Simplified superheterodyne receiver that employs the proposed high-performance down-converter mixer with CG, integrated filter, high LO to-RF/LO-to-IF isolation, and good input matching.

Table 2 Receiver cascaded noise analysis with a high-performance millimeter-wave mixer.

Component	Gain (dB)	Noise tem (K)	Cum. gain (dB)	T_{rx} (K)
HDPE window	−0.014	0.96	−0.014	0.96
Feed horn	−0.018	0.06	−0.032	1.02
OMT	−0.3	1.14	−0.332	2.16
Coupler	0	0.09	−0.332	2.26
WG to WG flange	−0.05	0.18	−0.382	2.46
LNA	30	13	29.618	16.60
WG to Coax Adpt.	−0.5	1.95	29.118	16.61
Steel cable	−2	87.7	27.118	16.71
CoaxCable to ND	−1	18.1	26.118	16.75
BPF	−2	175.4	24.118	17.18
Warm amplifier	25	495	49.118	19.09
Mixer	6	3000	55.118	19.12
Back-end cable	−5	648.6	50.118	19.13

wave ratio between amplifier and mixer. However, the proposed down-converter has high CG, high LO-to-RF isolation, and good input matching with an integrated IF filter, which allows for removing the isolator and extra IF amplifiers,[11] simplifying the system architecture as shown in Fig. 2(b).

Table 2 represents cascaded noise and gain analysis of the receiver for receiver architecture using a high-performance down converter.

1.2 Design Consideration

As discussed in Ref. 4 the backend requires a signal level of −25 to −20 dBm to operate properly. This corresponds to an accumulative gain of 50 dB considering an input signal from a black body with a temperature of 800 K. For a given low noise front end (cold + warm LNA), the architecture of the receiver is affected by the mixer's performance. Therefore, to be able to simplify the receiver architecture as a downconverter with at least 5 dB gain, 30 dB isolation, and input matching of at least 10 dB is required. Table 3 summarizes the mixer requirements.

This down converter is designed based on an IHP (innovations for high-performance Microelectronics, Frankfurt, Germany) silicon-germanium (SiGe) 130 nm process, which offers high-performance NPN heterojunction bipolar transistors (HBTs) with 300 GHz cut-off frequency and 500 GHz maximum oscillation frequency. The process also provides multi-layer metallization back end of line (BEOL) that allows for compact designs of complex millimeter-wave circuits.

2 Circuit Design

The fabricated chip demonstrates a measured single-ended CG of 5 to 8 dB (equivalent to 8 to 11 dB differential CG) with <3 dB variation and a low LO power of −6 dBm over the IF bandwidth of 8 to 16 GHz as the LO frequency range varies from 27 to 34 GHz, meeting the primary design goals. Furthermore, the test results show a wider RF frequency performance of 28 to 56

Table 3 Design specification for Q-band down converter.

Requirement	Value
CG (dB)	> 5
Gain flatness (dB)	2
RF frequency (GHz)	35 to 50
LO frequency (GHz)	27 to 34
IF frequency (GHz)	8 to 16
Input return loss (dB) (all ports)	≤ 10
LO-RF isolation (dB)	> 30
LO-IF isolation (dB)	> 30
RF-IF isolation (dB)	> 30
Output 1-dB compression (dBm)	≥ 20

GHz with 3 to 8 dB CG in the IF bandwidth of 6 to 18 GHz with the LO frequency of 22 to 38 GHz at an LO power of −5 dBm.

A measured LO-to-RF isolation >40 dB is achieved in addition to wideband RF port matching to 50 Ω, allowing to directly connect the down-converter to the postamplifier without the need of an isolator.

The entire down-converter chip consumes 80 mW power in a small size of 0.96 mm^2 including pads and chip streets, which is considerably smaller even when compared with stand-alone mixers.[13,15] The low LO drive power and DC power consumption of the mixer make it potentially integratable with a SiGe-based post-LNA (warm amplifier) operating at room temperature to further decrease the receiver size of the telescope's front-end.

Figure 3 shows the block diagram of the downconverter.

The down-converter block is designed based on a double-balanced Gilbert cell mixer,[16] which provides a better LO to RF/IF isolation compared with single-ended and single-balanced configurations. The double-balanced mixer requires differential RF and LO signals at the transconductor pair and the mixing quads, respectively. Thus, two on-chip transformer baluns at the RF and LO ports are used to convert the single-ended signals to differential ones. The mixer core is followed by a buffer stage that prevents the loading of the mixer by the next block. Finally, an on-chip filter blocks the LO and RF signals from leaking into the IF outputs.
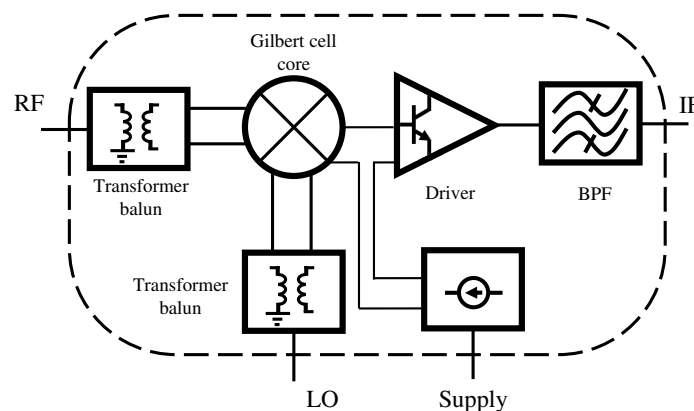
Fig. 3 Down-converter block diagram.

2.1 Mixing Core

In a Gilbert cell mixer core, shown in Fig. 3, where I_n corresponds the AC current of HBT Q_n, for the Q_3–Q_4 switching pair the difference between AC currents (blue arrows) can be obtained[17] as

$$\Delta I_{3,4} = I_3 - I_4 = I_1 \tanh\left(\frac{v_{LO}}{2v_{th}}\right),\qquad(1)$$

where v_{LO} is the differential LO signal at the base of Q_3 and Q_4, and v_{th} is the thermal voltage. Similarly, for Q_5–Q_6 pair the AC current difference equals

$$\Delta I_{5,6} = I_5 - I_6 = I_2 \tanh\left(\frac{v_{LO}}{2v_{th}}\right),\qquad(2)$$

and for the transconductor pair (Q_1–Q_2) the AC current difference is

$$\Delta I_{1,2} = I_1 - I_2 = I_{tail} \tanh\left(\frac{v_{RF}}{2v_{th}}\right),\qquad(3)$$

where I_{tail} is the total tail current, and v_{RF} is the differential RF voltage applied at the base of Q_1 and Q_2. The differential output voltage, v_{IF}, is

$$v_{IF} = \Delta I_{IF} R_L = [(I_3 + I_6) - (I_4 + I_5)]R_L = [\Delta I_{3,4} - \Delta I_{5,6}]R_L,\qquad(4)$$

where R_L is the load at the collector of the mixing quads. Replacing Eqs. (1)–(3) in Eq. (4) gives the large signal differential IF voltage

$$v_{IF} = R_L I_{tail} \tanh\left(\frac{v_{RF}}{2v_{th}}\right) \tanh\left(\frac{v_{LO}}{2v_{th}}\right).\qquad(5)$$

Assuming that the RF signal is small, Eq. (5) simplifies to

$$v_{IF} = R_L \frac{I_{tail}}{2v_{th}} v_{RF} \tanh\left(\frac{v_{LO}}{2v_{th}}\right).\qquad(6)$$

In the case where the LO signal is large enough, the tanh function can be approximated by the Fourier series of a square wave, and taking into account the frequency component at the desired IF frequency, the mixer CG is

$$CG = \frac{v_{IF}}{v_{RF}} = \frac{2}{\pi} R_L g_m,\qquad(7)$$

where g_m is the transconductance of Q_1 and Q_2, equals

$$g_m = \frac{I_{tail}/2}{v_{th}}.\qquad(8)$$

Considering the power budget, a 3.3-V standard power supply and a 16-mA tail current were used, and the transistor sizes were designed accordingly for the desired current density that provides high switching speed and low noise performance for the switching quad and transconductor pair, respectively.

Inductive loading provides a CG around the resonance frequency of the inductor and the capacitance of the output node, resulting in a narrow band performance. Therefore, a resistive loading is chosen over inductive to provide wideband performance (Fig. 4).

However, R_L and the tail current, and hence g_m, cannot be very large since the voltage drop across the resistor is limited, resulting in a relatively low gain. Therefore, considering the collector-emitter break-down voltage, the mixer is biased for maximum output swing, which results in about 400 mV voltage drop across R_L. The main linearity constraint is imposed by the input swing that is very limited due to the fact that the voltage at the base of the transconductor pair
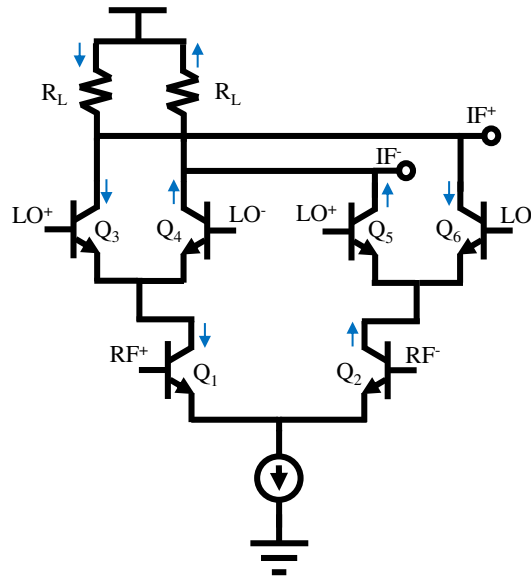
Fig. 4 Mixer core schematic. Q_1 and Q_2 are the transconductor pair. Q_3, Q_4, Q_5, and Q_6 are the switching quad. Arrows show the AC currents.

cannot swing more than a few mV without the collector current, as described by Eq. (3), showing a nonlinear dependence to v_{RF}. This results in a voltage saturation across the load, and the linear region is only a few mV wide, about $v_{th} = 25$ mV. To improve the input swing problem, an inductor can be added at the emitter of the transconductor pair.[17] The degeneration allows the AC voltage of the emitter to be a nonzero value. Thus, the HBT can tolerate a larger swing at the input. This largely improves the 1-dB input compression point as well as the input impedance match. The major drawback of this approach is reducing the effective g_m and causing a lower CG. Further degeneration could increase the input 1-dB compression, but the CG will become negative and the linearity becomes limited by the output swing at the IF.

Figure 5 shows the simplified schematic of the down converter where an emitter follower is placed between the mixer output and the band pass filter to act as a buffer and reduce the loading of the mixer. The diodes at the collector of the emitter followers are diode-connected HBTs that shift the V_{dd} to a lower level to prevent the break-down of transistors.

The emitter followers have a current source at the emitters. An inductor is placed at the emitter of current source devices to further increase the output impedance seen at the collector of the current source without changing the DC operation point.

The bias circuit shown in Fig. 5 provides the required voltages for the mixer core. The resistor between the collector of QB_1 and the emitter of QB_2 (QB_1 and QB_2 are current mirror bias
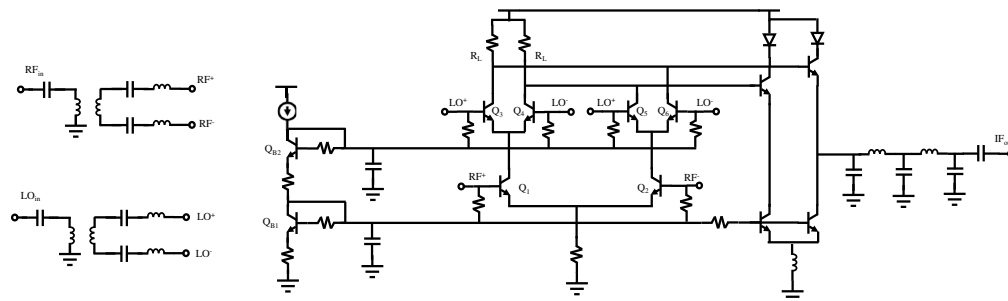
Fig. 5 Simplified schematic of the down converter. The transformer balun and matching network for RF and LO are shown at the left side. Current mirror devices (QB1 and QB2) to generate the required base-emitter voltage for the transconductor pair (Q_1 and Q_2) and switching quad (Q_3, Q_4, Q_5, and Q_6), respectively, the driver buffer (Q_7 and Q_8) and their tail current source (Q_9 and Q_{10}) shown at the right side.

transistors) in the bias circuit provides a voltage drop that allows for some headroom at the collector of the transconductor pair, thus allowing a larger swing. The resistor added at the collector of QB_2 allows the use of the standard 3.3-V supply voltage.

2.2 Passive Component Analysis

Modern SiGe HBT technologies allow the integration of high-performance RF modules together on a single die. However, the performance of high-frequency RF systems is also largely determined by their passive components, signal transmission lines, and interconnections. An optimum design of passive structures with a high-quality factor is critical for low loss and high gain at millimeter-wave frequency. To capture the effect of the BEOL interconnection on the device performance, a 3D model of the metals and vias was developed. Normally, the device parameters provided by semiconductor foundries include the intrinsic device plus the first interconnect metal layer, and the rest are de-embedded. Therefore, it is critical to model the parasitic effects of the interconnections with access terminals at the top metal layers for millimeter-wave circuits. For this purpose, two versions of the interconnection were designed as shown in Fig. 6. The one in Fig. 6(a) utilizes wider metals to reduce the access resistance in the expense of the higher parasitic capacitance and the other, in Fig. 6(b), employs narrow tracks that have less parasitic capacitance and allow for the higher cut-off frequency at the expense of high resistance resulting in higher minimum noise.

These structures were fully simulated, without via array simplification, using the keysight advanced design system (ADS) finite element method (FEM) simulator. Figure 7 shows the insertion loss as well as the phase of the transition between the device contact metal and the top-metal terminals for low noise, Fig. 6(a), and for high-speed Fig. 6(b). The former utilizes wider connections with more via counts that reduce the access resistance, making it a suitable choice for devices that are operating in low noise conditions.

However, the parasitic capacitances of the interconnections reduce the cut-off frequency of the device by 20%, as shown in Fig. 8, compared with a device without the metal interconnections. The increase in minimum noise figure is 0.15 dB at 60 GHz. The latter, used in this design, is a high-speed version where narrower interconnects are used to reduce the parasitic capacitance

(a)　　　　　　　　　　　(b)
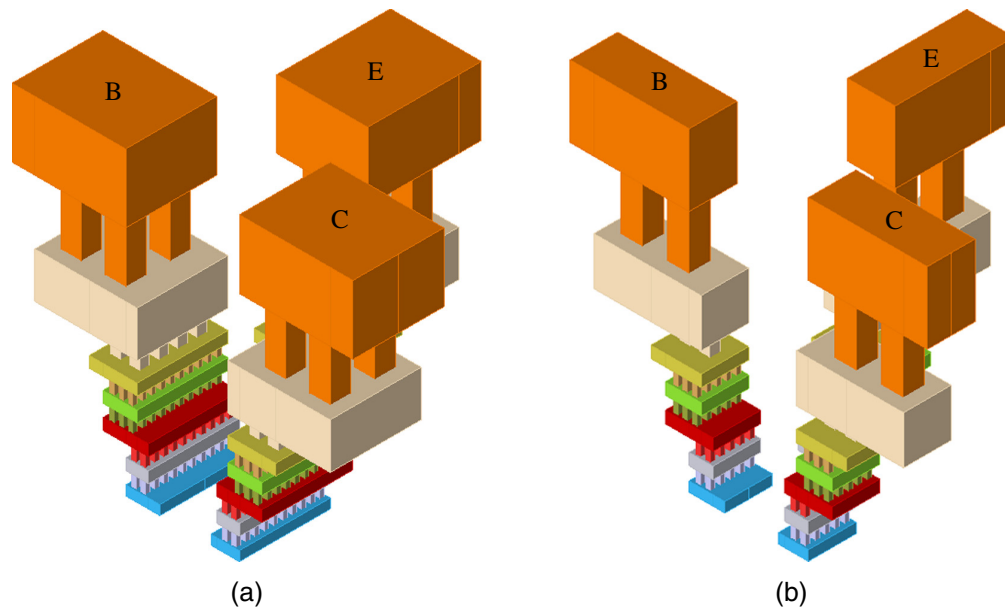
Fig. 6 3D representation of a device metal interconnection for (a) wider tracks and double numbers of vias for lower loss and noise with larger parasitic capacitance and (b) narrower tracks and less number vias resulting in less parasitic capacitance and wider bandwidth in the expense of higher loss. Base, emitter, and collector terminals of the HBT are labeled with B, E, and C, respectively.
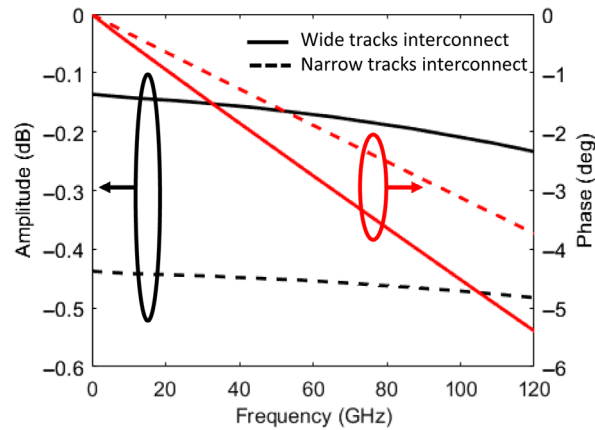
Fig. 7 Simulated amplitude and phase of the transition between lower metal and top metal interconnect for the base of the HBT for low noise (solid line) and high speed (dashed line) interconnections. Low noise interconnect provides 0.3 dB less loss compared with high speed interconnect.
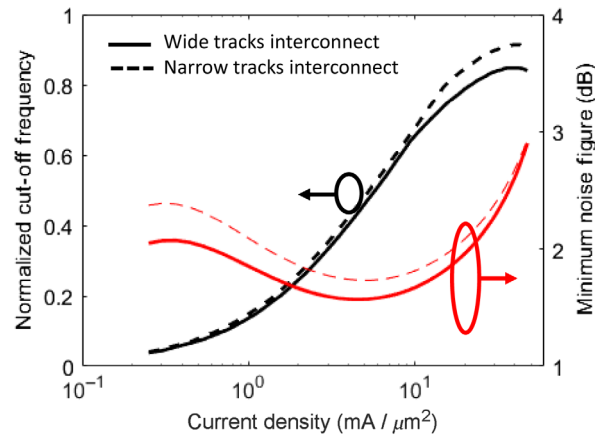
Fig. 8 Simulated cut-off frequency (normalized to maximum cut-off frequency of the transistor without metal interconnect) and minimum noise figure (at 60 GHz) for a device with low noise (solid line) and high speed (dashed line) interconnects. The high speed interconnect shows less degradation in the cut-off frequency compared with the intrinsic device (device without interconnect).

and preserve the cut-off frequency, with only a 10% reduction in maximum cut-off frequency. This leads to higher resistance and 0.32 dB increase in minimum noise figure of the device at 60 GHz compared with a bare transistor as shown in Fig. 8. Figure 9(a) shows the transmission and bias line structure used in this work. The supply voltage is distributed using wide tracks with a low impedance that are shielded by ground planes and walls.

The base bias lines are at the lower narrow metal layers with high impedance and proper shielding. The transmission lines (TMs) are realized by using grounded coplanar waveguide (GCPW) structures with a 6-7-6 μm G-S-G structure on the top metal, providing 50 Ω signal lines. Figure 9(b) depicts the simulation results of the GCPW line with <1 dB/mm loss at 70 GHz.

2.3 *Layout Optimization*

In the topology of a double balanced mixer, two signal line cross-overs, at least, among RF, IF, and LO are inevitable in the core layout. This phenomenon as well as the parasitic coupling between adjacent tracks are the main limiting factors of the isolation. To minimize the coupling, the tracks are designed to have orthogonal current wherever possible. Figure 10 shows the 3D

(a)

(b)
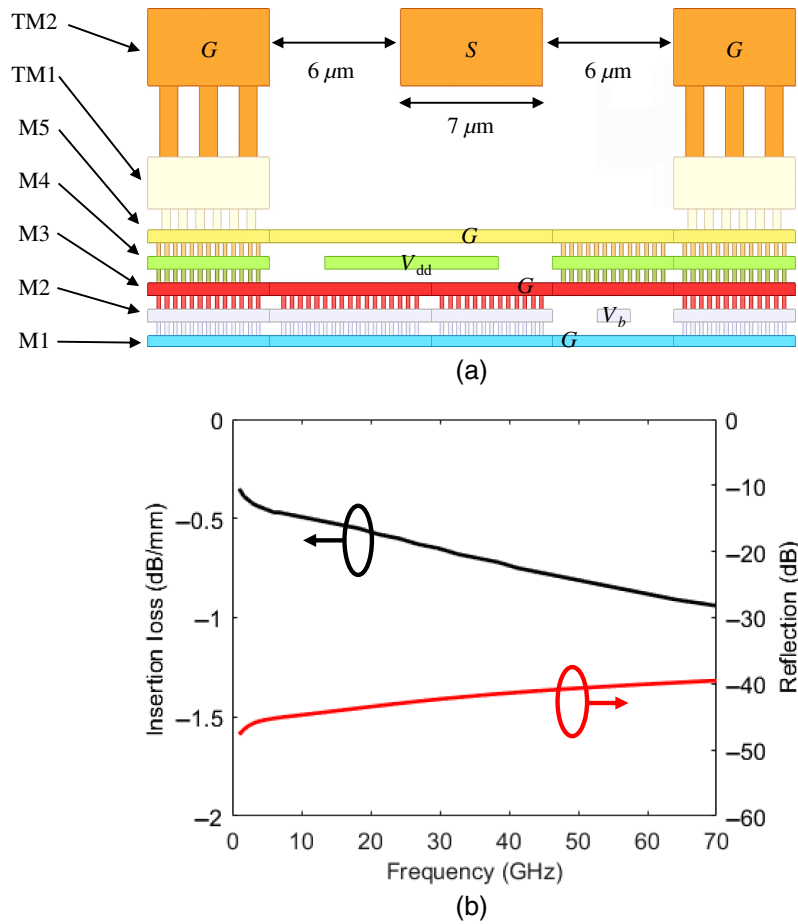
Fig. 9 (a) Interconnection stack-up of GCPW transmission line made of TM2 as signal (S) line and M5 as ground (G) with sidewalls made of TM2, TM1, M5, and vias. The bias lines are realized in M4 and M2 layers (b) simulated performance of the GCPW. The transmission line provides low loss at millimeter-wave frequencies.
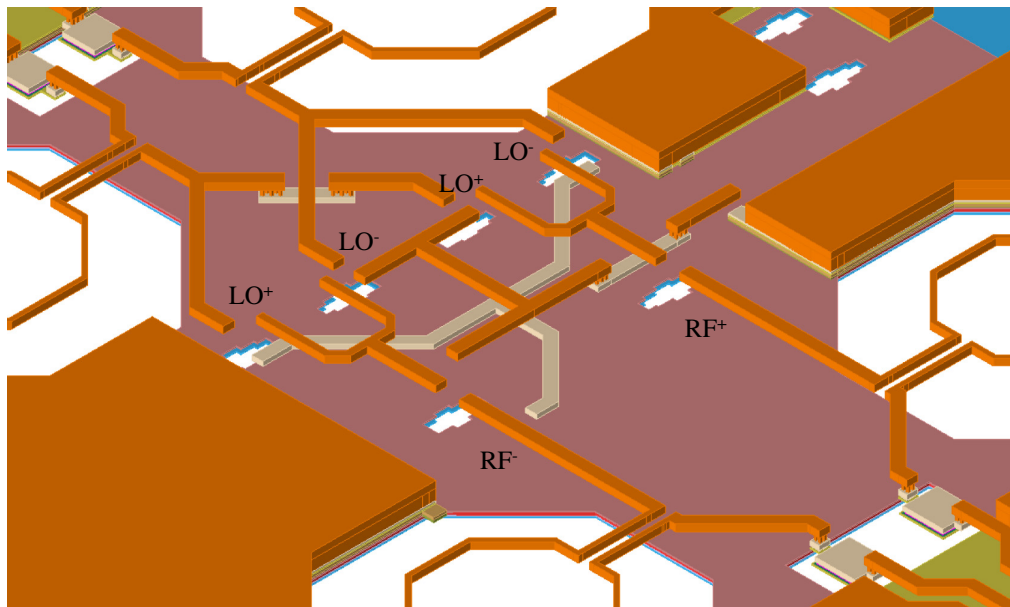
Fig. 10 3D layout model of mixer core interconnect. RF and LO lines are placed on either side of the layout to minimize coupling and orthogonal alignment of RF and IF reduce the coupling and increase the isolation.

(a)

(b)
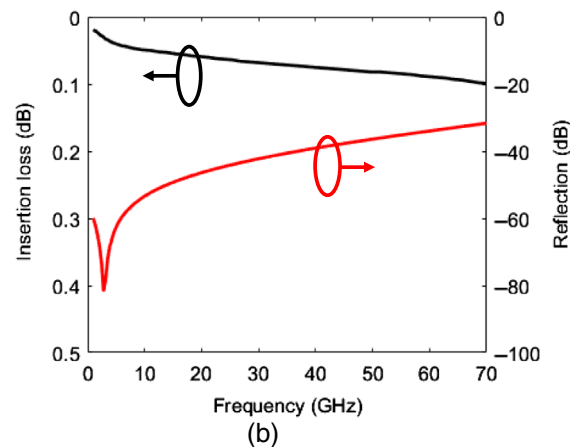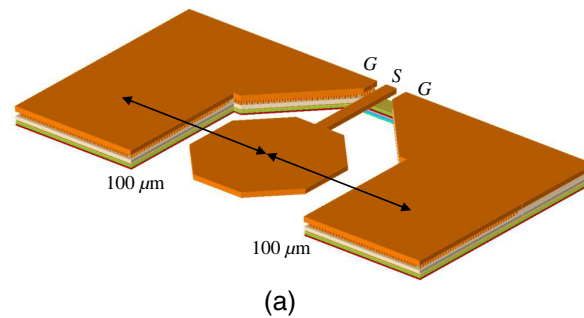
Fig. 11 (a) 100-μm ground-signal-ground (GSG) transition to GCPW the tapered ground plane allows to achieve minimum reflection where the inductance of the short narrow line cancels out the pad capacitance for wider frequency performance and (b) simulation results of the 100 μm GSG transition to GCPW.

layout model of the core where RF and LO signals are fed from opposite directions to minimize the RF-LO leakage. Also, all the transformers and inductors are separated with ground planes.

To minimize the effect of bonding pads on the performance of the chip, the connection to GCPW, shown in Fig. 11(a), was optimized for a 100-μm pitch GSG. Figure 11(b) presents the simulated GSG transition using FEM. The tapered ground location was chosen to provide low insertion loss and wideband match to 50 Ω up to 60 GHz. The simulation shows the reflection coefficient $S_{11} < -30$ dB and transmission coefficient $S_{21} > -0.1$ dB over the frequency of interest.

To convert the single-ended input signals to differential ones, two on-chip transformer baluns were designed using the two thick top metal layers. As shown in Fig. 5, they are codesigned with the input matching network for RF and LO ports. As shown in Fig. 12, both transformers have a 1:1 turn ratio and are better than 0.6 and 0.8 dB amplitude and 1.5 deg and 2 deg phase balance for RF and LO baluns, respectively.

An offset in the diameter of the primary and secondary coils is applied to improve the frequency performance by reducing the capacitive coupling between metal tracks. Also, it helps to reduce the amplitude imbalance by compensating for the difference in the resistive loss of the coils caused by different metal thicknesses.

Prior to connecting to the output pad, a fifth-order LC Butterworth type filter with a decoupling capacitor and having 30 dB attenuation in the stop band above 24 GHz, as depicted in Fig. 5, is placed at the IF port. Note that one of the deferential IF signals is routed to the output.

Figure 13 shows the microphotograph of the fabricated chip with a size of 0.8×1.2 mm^2.

3 Measured Results

Figure 14 shows the measurement set up used to characterize the chip on an RF probe station. A Keysight PNA 5227B with frequency offset (this option allows for mixer measurements using

(a)   (b)
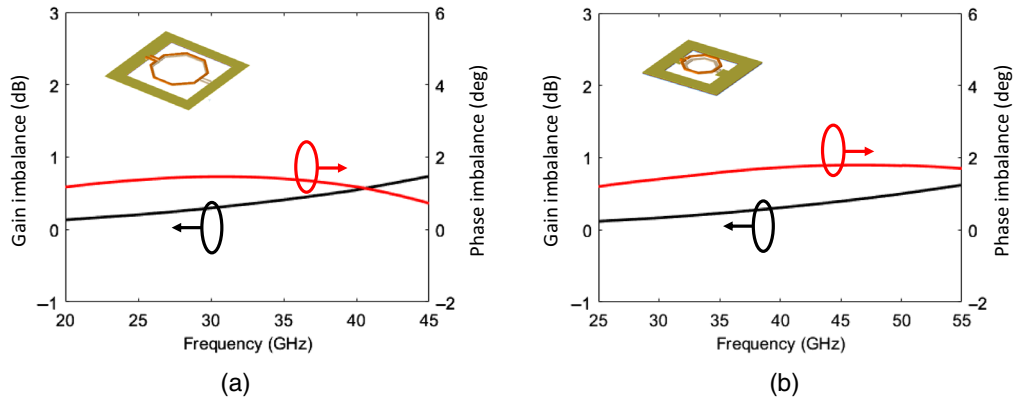
Fig. 12 Simulated performance of the (a) LO transformer and (b) RF transformer baluns providing <0.5 dB and 2-deg amplitude and phase imbalance, respectively, result in low LO leakage to RF and IF.
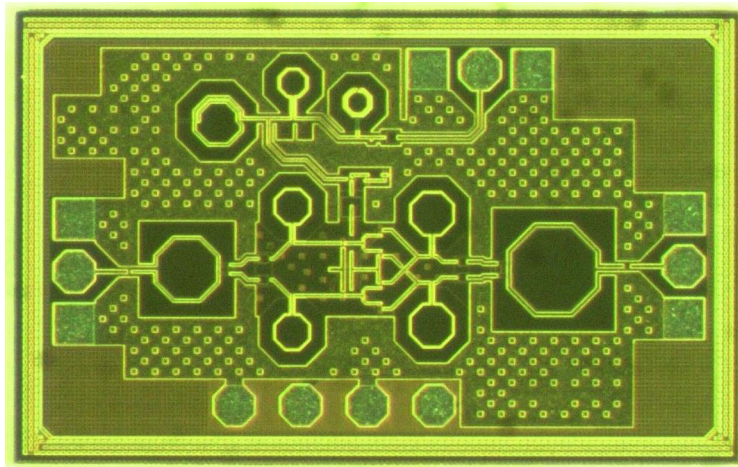
Fig. 13 Microphotograph of the down-converter chip with a size of 0.8×1.2 mm^2. RF Pad is located at left side, LO pad is on the right side, the IF is located on the top and the bias pads are at the bottom of the chip.
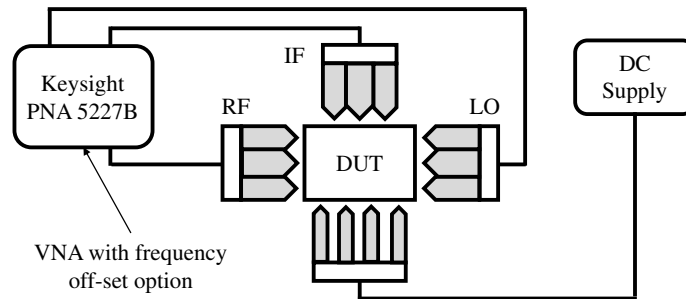
Fig. 14 RF-Probe Station measurement setup of the device under test using a four-port VNA with frequency off-set option.

a single vector network analyzer (VNA) with two signal sources that operate at different frequencies and four ports were used to measure the S-parameters, CG, and isolations. Figure 15 shows the measured input reflection coefficient at three ports with a three-port short-open-load-thru (SOLT) calibration. All three ports have < -10 dB matching over the frequencies of interest, and the circuit is stable over the frequency range of measurements (10 MHz to 60 GHz).
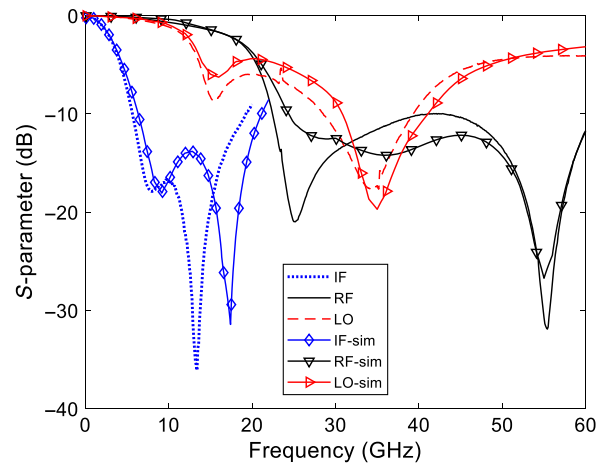
Fig. 15 Simulated (dashed) versus measured (solid) input reflection of the down-converter ports.
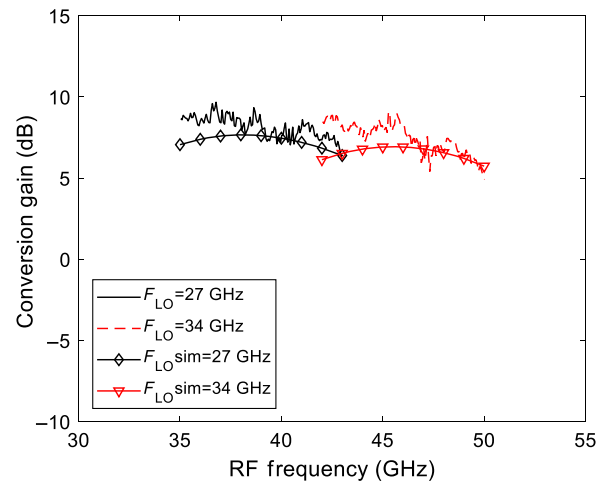
Fig. 16 Simulated (dashed) versus measured (solid) down-converter CG for two RF sub-bands with 8 to 16 GHz IF.

Figure 16 shows the measured CG of the mixer for two sub-band LO frequencies with an IF of 8 to 16 GHz under an LO power of −6 dBm and nominal RF power of −30 dBm. An 8 dB CG was measured with 3 dB gain flatness in the 8 to 16 GHz IF range. Figure 17 presents the CG over the IF bandwidth of 6 to 18 GHz, which is 4 GHz wider than the original design requirement of 4 to 8 dB CG. This corresponds to 33 to 52 GHz RF bandwidth. Also, the RF frequency can be expanded from 35 to 50 GHz and 28 to 56 GHz if lower CG is acceptable as shown in Fig. 18. The measured gain shows a faster drop with respect to frequency mainly due to larger metal loss at higher frequencies.

Figure 19 shows the measured isolation between the LO and the other two ports. Note that the LO to IF leakage is ≤ 30 dB, a better performance compared with the −25 dB predicted from simulated results. Figure 20 demonstrates that the RF leakage to IF isolation is higher than 40 dB. And the RF to LO isolation is better than 30 dB over most of the bandwidth.

In practice, the metal loss at higher frequencies is larger, which further attenuates the leaked signal at from one port to another.

For the CG compression test, the LO frequency was set at 30 GHz with −6 dBm power, and the RF power of a 48-GHz signal was swept. Figure 21 shows the CG change with respect to RF input power. It depicts the IF output power as a function of the input RF power. The 1 dB compression point occurs at −14 dBm input power and corresponds to a −10 dBm output swing, which is in agreement with simulation results.
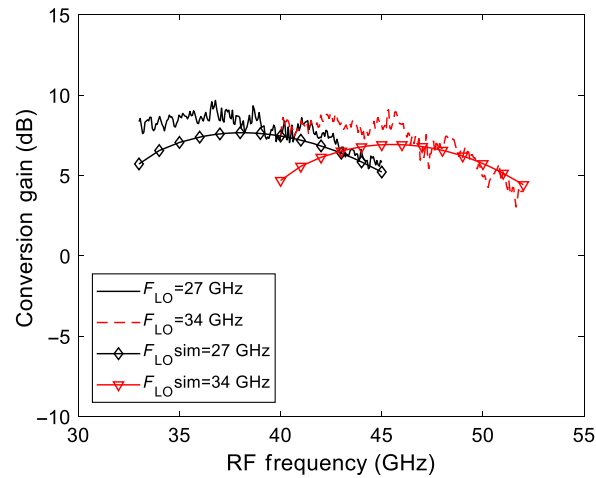
Fig. 17 Simulated (dashed) versus measured (solid) down-converter CG with a wide IF of 6 to 18 GHz.
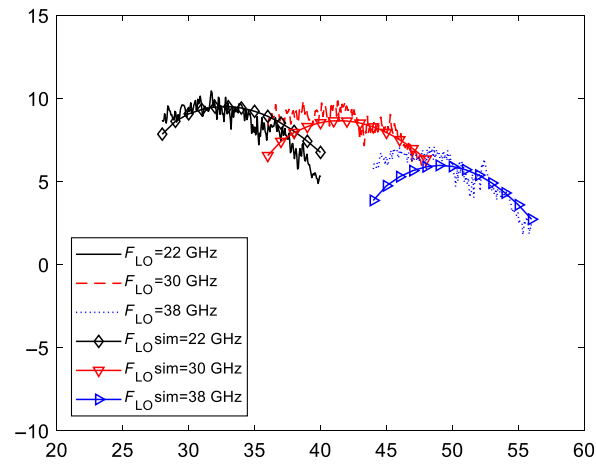
Fig. 18 Simulated (dashed) versus measured (solid) down-converter CG for a wideband RF of 28 to 56 GHz.
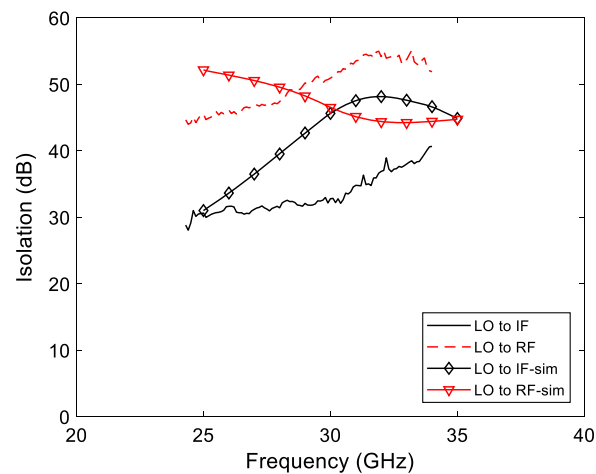
Fig. 19 Simulated (dashed) versus measured (solid) isolation of the down-converter from LO to IF and RF.
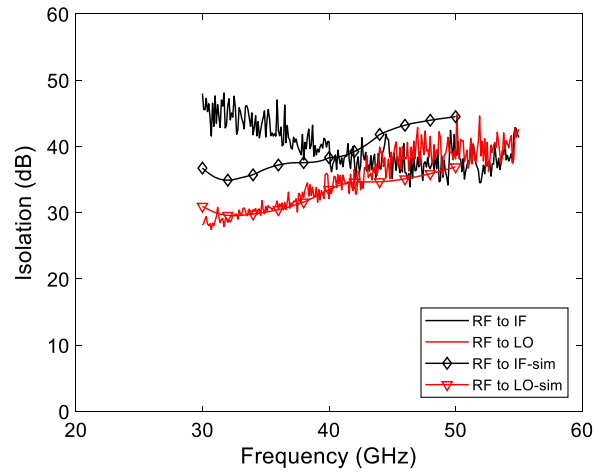
Fig. 20 Simulated (dashed) versus measured (solid) down-converter RF to IF and LO isolation.
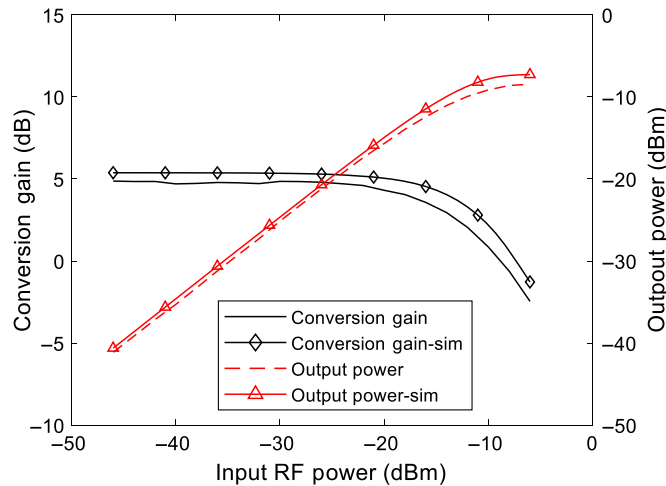
Fig. 21 Simulated (dashed) versus measured (solid) down-converter CG compression and output power; at RF = 48 GHz, LO = 30 GHz, and LO power = −6 dBm.

The downconverter is able to provide conversion "gain" with an LO power as low as −12 dBm, which greatly relaxes the LO generation and distribution requirements regarding the circuit complexity, component count, and power consumption.

Table 4 summarizes the down converter performance in comparison with published mixers for radio astronomy applications in similar frequency bands. This work demonstrates high CG, high LO-to-RF and LO-to-IF isolation, and the lowest LO power requirement.

4 Conclusion

High-performance SiGe HBT technology provides a platform for a complex system in milli-meter-wave applications. High integration of transistors and passive components is a challenge at millimeter-wave frequencies. Accurate characterization of passive components and transmis-sion networks including the metal stack is critical for wideband impedance matching and achiev-ing optimum transistor performance. The multifunction circuit blocks of a double balanced mixer core, two baluns, IF buffer, and bandpass filter are optimized and fully EM simulated with FEM. The design results agreed well with the measured module performance such as wide-band frequency (28 to 56 GHz), high CG (8 dB), low LO operation (−6 dBm), good return losses ≤ 10 dB at RF/LO/IF ports, and LO-to-IF/LO-to-RF/RF-to-IF isolations >30 dB/40

Table 4 Summary of published Q-band mixer performances. For standard band (35 to 50 GHz) and wideband (28 to 56 GHz).

Ref.	Technology	RF Freq. (GHz)	IF Freq. (GHz)	CG (dB)	LO/RF ISO (dB)	LO/IF ISO (dB)	LO power (dBm)	Size (mm²)	Power (mW)
18	GaAs pHEMT	32 to 52	2 to 12	4 to 7	38	35	4	2	NA
19	180 nm SiGe	50 to 067	0.5 to 8.5	13	NA	NA	3	0.146	66
14	90 nm CMOS	30 to 90	DC-20	−7.5	>30	NA	2.5	0.389	0.6
9	150 nm GaAs pHEMT	34 to 53	3 to 13	−2	>37	>21	0	2.25	36
This work	SiGe HBT	35 to 50	8 to 16	5 to 8	>42	>30	−6	0.96	80
		28 to 56	6 to 18	3 to 8					

dB/35 dB, respectively. The entire down conversion module consumes 80 mW DC power with a single 3.3-V bias supply. This compact down-converter module is suitable for the Q-band radio telescope receiver application. The chip will be packaged in a custom-designed chassis described in Ref. 5 to be integrated with the receiver front end. The packaging of such chip is challenging due to the absence of a back metallization (in contrast to GaAs chips with back side metallization). The ground for high-frequency signals are defined on the surface of the chip, hence wire bonds are required for connecting the ground pads to the chassis ground. This work demonstrates the capability and advantage of employing SiGe HBT technology for designing high-performance millimeter-wave down-converters with wide bandwidth that are integrated with more components to reduce the system complexity and cost. National Research Council Herzberg Astronomy and Astrophysics is planning to extend this design methodology to direct conversion mixers for near future instruments such as ngVLA band 5 and band 6.

Acknowledgments

References

1. "Atacama large mm-wave array," http://www.almaobservatory.org (2022).
2. "Next generation very large array," http://ngvla.nrao.edu/ (2022).
3. M. Islam and G. Lacy, "An improved secondary reflector for DVA-2 radio telescope: a case study on application of structural optimization technique," *Proc. SPIE* **10700**, 107005T (2018).
4. L. Locke et al., "Q-band single pixel receiver development for the ngVLA and NRC," *Proc. SPIE* **10708**, 1070832 (2018).
5. S. Salem Hesari et al., "Q-band receiver system design for the Canadian DVA-2 radio telescope," *Proc. SPIE* **11453**, 114533A (2020).
6. R. J. Selina et al., "ngVLA system reference design, Volume 1," ngVLA Document 020.10.20.00.00-0001-REP-B-SYSTEM_REFERENCE_DESIGN (2019).
7. H. Y. Yang et al., "Design and analysis of a 0.8–77.5-GHz ultra-broadband distributed drain mixer using 0.13-μm CMOS technology," *IEEE Trans. Microwave Theory Technol.* **57**(3), 562–572 (2009).

8. J. Tsai, "Design of 40–108-GHz low-power and high-speed CMOS up-/down-conversion ring mixers for multistandard MMW radio applications," *IEEE Trans. Microwave Theory Technol.* **60**(3), 670–678 (2012).
9. P.-C. Huang et al., "A compact 35-65 GHz up-conversion mixer with integrated broadband transformers in 0.18-μm SiGe BiCMOS technology," in *Proc. IEEE Radio Freq. Integr. Circuits Symp.*, San Francisco, California, pp. 1–4 (2006).
10. C. Chen et al., "A high LO-to-RF isolation 34–53 GHz cascode mixer for ALMA observatory applications," in *IEEE/MTT-S Int. Microwave Symp. Dig.*, Philadelphia, Pennsylvania, pp. 686–689 (2018).
11. J. Tsai and T. Huang, "35–65-GHz CMOS broadband modulator and demodulator with subharmonic pumping for MMW wireless gigabit applications," *IEEE Trans. Microwave Theory Technol.* **55**(10), 2075–2085 (2007).
12. Y. Hwang, C. Han, and Y. Huang, "A photonic-tunable cryogenically cooled W-band subharmonically-pumped GaAs HEMT diode mixer module," in *Proc. Eur. Microwave Integr. Circuits Conf.*, Rome, pp. 208–211 (2009).
13. S. Weng et al., "A 35–50 GHz triple cascode mixer module with intermediate frequency of 4–12 GHz based on low noise GaAs PHEMT process," in *Proc. IEEE Int. Symp. Radio-Freq. Integr. Technol.*, Taipei, pp. 1–3 (2016).
14. Y.-C. Wu et al., "A novel 30–90-GHz singly balanced mixer with broadband LO/IF," *IEEE Trans. Microwave Theory Technol.* **64**(12), 4611–4623 (2016).
15. Y.-C. Wu et al., "An innovative joint-injection mixer with broadband IF and RF for advanced heterodyne receivers of millimeter-wave astronomy," *IEEE Trans. Microwave Theory Technol.* **68**(12), 5408–5422 (2020).
16. B. Gilbert, "A precise four-quadrant multiplier with subnanosecond response," *IEEE J. Solid-State Circuits* **3**(4), 365–373 (1968).
17. S. Voinigescu, *High Frequency Integrated Circuits*, Cambridge University, Cambridge, U.K. (2013).
18. J. Kao et al., "A high LO-to-RF isolation 32–52 GHz triple cascode down-conversion mixer with 2–12 GHz IF bandwidth for ALMA band-1," in *Proc. Asia-Pac. Microwave Conf.*, Sendai, pp. 1190–1192 (2014).
19. J. A. Qayyum, J. D. Albrecht, and A. C. Ulusoy, "A compact V-band upconversion mixer with −1.4-dBm OP1dB in SiGe HBT technology," *IEEE Microwave Wireless Comp. Lett.* **29**(4), 276–278 (2019).

Alireza Seyfollahi is an MMIC/RFIC in National Research Council Herzberg Astronomy and Astrophysics Research Center in Victoria, B.C., Canada. His research interest is design and development of high-frequency integrated circuit such as low-noise amplifiers and down-converter mixers for radio telescopes. He is a PhD student in the Electrical and Computer Engineering Department University of Victoria. His research is focused on development of millimeter-wave integrated circuits.

Nianhua Jiang is a senior research engineer at National Research Council Herzberg Astronomy and Astrophysics Research center in Victoria, B.C., Canada. His expertise is low-noise amplifier and radio astronomy receiver design. He has been working on microwave and millimeter-wave integrated circuits, transistor modeling, noise analysis, and microwave measurement. He has worked on ALMA band 3 receiver MeerKAT LNA and square kilometer array band 2 receiver.

Lewis B. G. Knee is the radio instrumentation team leader in National Research Council Herzberg Astronomy and Astrophysics Research center in Victoria, B.C., Canada. His experts are radio and (sub) millimeter astronomy, radio telescope instrument and system test and commissioning and studies of Galactic interstellar medium. He has 61 referred journal publications in astronomy and physics, 18 in radio astronomy technology, 82 scientific and technical reports, and 462 system integration test reports for ALMA.

Jens Bornemann is a professor in the Department of Electrical and Computer Engineering, University of Victoria, B.C., Canada. His research includes RF/wireless/microwave/millimeter-wave components and systems design, field-theory-based modeling of integrated circuits, feed

networks, and antennas. He authored/coauthored more than 350 technical papers. He is a Registered Professional Engineer in the Province of British Columbia, Canada, a Fellow IEEE, a Fellow of the Canadian Academy of Engineering, and a Fellow of the Engineering Institute of Canada.